Pertanika J. Sci. & Technol. 30 (4): 2333 - 2362 (2022)

PERTANIKA JOURNALS

SCIENCE & TECHNOLOGY

Journal homepage: http://www.pertanika.upm.edu.my/

Evaluation of Subcritical Organic Rankine Cycle by Pure and Zeotropic of Binary and Ternary Refrigerants

Omid Rowshanaie[1], Mohd Zahirasri Mohd Tohir[1]*, Faizal Mustapha[2], Mohammad Effendy Ya'acob[3] and Hooman Rowshanaie[4]

[1]Department of Chemical and Environmental Engineering, Universiti Putra Malaysia, 43400 UPM, Serdang, Selangor, Malaysia
[2]Department of Aerospace Engineering, Universiti Putra Malaysia, 43400 UPM, Serdang, Selangor, Malaysia
[3]Department of Process and Food Engineering, Universiti Putra Malaysia, 43400 UPM, Serdang, Selangor, Malaysia
[4]Department of Crop Science, Universiti Putra Malaysia, 43400 UPM, Serdang, Selangor, Malaysia

ABSTRACT

The simulation configuration and process analysis of the Subcritical Organic Rankine Cycle (SORC) system are carried out for the potential comparison between pure, binary, and ternary zeotropic mixtures of R1234ze(E), R1234yf, and R134a as refrigerant working fluids based on applying the flue gas as a heat source with medium temperature. The compression pressure was selected as an optimized variable input parameter of SORC with the lower limit of boundary condition (1.4 MPa); to mitigate air ingress and sub-atmospheric pressure that led to approach optimum net power output generated. Increasing the compression pressure has a positive relationship with the superheated temperature and the mass enthalpy change in the evaporation and, therefore, in the expansion process. In parallel, the enthalpy and entropy changes in the flue gas and cold water positively correlate with exergy efficiency. So, R1234ze(E)/R1234yf/R134a with 68.35% and R1234yf/R134a with 69.29% as the lowest and highest exergy efficiency in the highest compression pressure; furthermore, the SIC consequences of increasing the cost of each component of the SORC system that has a direct relationship with the PPC and the required exchanger area of evaporation and condensation process and generating a net power output of the turbine. As a result, the maximum to the minimum value of specific

ARTICLE INFO

Article history:
Received: 13 January 2022
Accepted: 05 April 2022
Published: 21 July 2022

DOI: https://doi.org/10.47836/pjst.30.4.02

E-mail addresses:
omid.rowshanaie@gmail.com (Omid Rowshanaie)
zahirasri@upm.edu.my (Mohd Zahirasri Mohd Tohir)
faizalms@upm.edu.my (Faizal Mustapha)
m_effendy@upm.edu.my (Mohammad Effendy Ya'acob)
hooman.rowshanaie@gmail.com (Hooman Rowshanaie)
* Corresponding author

ISSN: 0128-7680
e-ISSN: 2231-8526

investment cost (SIC) achieves R134a with 5807402.18-22455670.61 $.kW^{-1} and R1234yf with 16.82-17.38% reduction, respectively. To sum up, the lowest payback period (PBP) was R1234yf with 302 days.

Keywords: Exergy efficiency, flue gas, Organic Rankine Cycle (ORC), payback period (PBP), specific investment cost (SIC)

INTRODUCTION

Power and the environment are the two major concerns of this era. The aggravated usage of non-renewable energy sources, especially fossil fuels, has a destructive effect on the environment. It can create climate change and air pollution, cause acid rain, ozone depletion, carbon footprint, greenhouse gases emission effect, and global warming (F. Wang et al., 2021; Z. Wang et al., 2021; Lu et al., 2021; K. Sun et al., 2021; Q. Sun et al., 2021; Ping et al., 2021). However, applying low to medium temperature of waste heat source temperature (<350 ℃) reveals that more than 50% of industrial waste heat by driving several waste heat recovery applications can reduce these harmful environmental obstacles and, on the other hand, able to convert these waste heat source into power (Alvi et al., 2021a; Yu et al., 2021; Zhang et al., 2020; Ahmadi et al., 2020; Li et al., 2017; Li et al., 2018; Vélez et al., 2012; Peris et al., 2015; Imran et al., 2018).

Nowadays, the Organic Rankine Cycle (ORC) applications among the various waste heat recovery applications as a most promising and prospective technology are selected to convert low to medium temperature of heat sources, including geothermal energy, biomass energy, solar thermal energy, and industrial waste heat especially flue gas into power (Schilling et al., 2021; Kavathia et al., 2021; Loni et al., 2021; Alvi et al., 2021b; Eyerer et al., 2020; Vaupel et al., 2021; Hamid et al., 2021).

In general, some scholars attempt to investigate and utilize the new, green, and environmentally friendly refrigerant organic working fluids in ORC based on the very low GWP (GWP<1), ODP with zero amount, and more suitable safety grading, low boiling point, and low atmospheric lifetime. Roumpedakis et al. (2020) studied the small-scale ORC system by using a solar as a low-temperature heat source and analysis and fulfillment by applying different typical organic refrigerant working fluids such as R134a, R245fa, R152a, R237ea, R236ea beside a new and environmentally friendly refrigerant working fluid like R1234ze(E) and investigating on the exergy efficiency, thermal efficiency, and thermo-economic parameters. In conclusion, apart from R245fa with the highest exergy and thermal efficiency, the short payback period belonged to a new and environmentally friendly working fluid, R1234ze(E). Molés et al. (2017) considered the performance of an ORC system driven by R1234yf and R1234ze as two working fluids with low GWP and alternative to an old working fluid, R134a, based on a varied range of evaporating

temperatures and condensing temperatures. The results depict that R1234yf would consume higher pump power as a power input compared with R134a by 18.3% to 25.8%.

Furthermore, in various evaporating and condensing temperatures, R1234ze has the highest trend of net cycle efficiency among R1234yf and R134a. Ata et al. (2020) optimized and analyzed an ORC system driven by R1234ze as a new-generation fluid using a heat source with 120°C. The current study performed six performances: thermal efficiency, turbine power, exergy efficiency, total irreversibility, Volume Flow Ratio (VFR), and Environmental Effect Factor (EEF) using the orthogonal design with Taguchi-ANOVA. The main control factors were $\Delta T_{PP,e}$- $\Delta T_{PP,c}$-$T_{c,i}$-T_{sup}- η_t- η_p selected for the statistical analysis. EES's numerical analysis showed that the implemented sensitivity level ranking maximizes thermal efficiency as isentropic efficiency of the turbine, η_t (33.64%). Nevertheless, the scale of sensitivity levels to optimize turbine performance was analyzed as the inlet temperature of cooling water as a heat sink, $T_{c,i}$ (65.21%). Li et al. (2017) focused on the new-kind environmentally friendly, green, and safe organic refrigerant working fluid, R1234ze(E), as a considerable potential to be applied in subcritical and transcritical ORC applications used by the hot water as a heat source with 100–200 °C inlet temperature and no restriction of outlet temperature limit. Therefore, two of the optimized parameters in the expansion process were the inlet pressure and temperature of the turbine. In a nutshell, in this study, the highest system net power output of R1234ze(E) in comparison with R600a and also R245fa at 100–167 °C heat sources with no restriction of outlet temperature was maximum with 31.4% and 25.8% larger than that of R245fa and R600a, respectively.

In addition to paying attention to the new and environmentally friendly refrigerant organic working fluids in ORC, the main working conditions, especially subcritical besides transcritical, are carried out by particular groups of researchers, which are in parallel with the current study. Zhang et al. (2018) selected a subcritical as a working condition of air-cooled ORC using the 150 °C as a low-temperature geothermal brine. This research focused on applying R245fa as the typical working fluid. Also, R1234ze(E) and R1234ze(Z) were two low ODP and GWP working fluids to reach the maximum exergy efficiency main achievement of the system. These scholars exposed that, for 100 kg/s geothermal sources, the highest and maximum exergy efficiency of the system besides the highest total efficiency of the system between these typical and low GWP and zero ODP organic refrigerant working fluids belonged to an environmentally friendly and new working fluid, R1234ze(E) in the chemical process industry (CPI). Another research in the case of subcritical working conditions is Yang et al. (2015). They considered the choice of the most suitable working fluid for an ORC in terms of subcritical working conditions and made a comparison between several typical and new environmentally friendly working fluids, including R600, R600a, R601a, R245fa beside R1234ze and R1234yf and also utilizing a heat source such as the diesel engine with 200–370 °C as an exhaust waste heat recovery application. They achieved

that after analyzing and investigating all of the working fluids that drive this subcritical ORC (SORC), R1234ze(E) was chosen as a significant thermodynamic performance. Chagnon-Lessard et al. (2020) performed different numerical tools of a geothermal ORC, which was driven by 20 other potential typical and new environmental friendly working fluids; and (ORC/S/SC) as the subcritical ORC using the single-pressure heater, (ORC/S/TC) as the transcritical ORC using the single-pressure heater, (ORC/D/SC) as the subcritical ORC using the dual-pressure heater. Last but not least was (ORC/D/TC) as the transcritical ORC using the dual-pressure heater. Furthermore, the specific work output was chosen as an objective function of this SORC system, and some variables, such as work pressures, the brine, the working fluid mass flow ratios, effectiveness of superheaters, and the range of the cooling tower, were chosen in this study. Their main achievement was among the 20 working fluids of this research, R1234yf, R115, R125, R218, R227ea, R134a, R22, R124, R32, RC318, R134a, R12, RE245cb2, and R152a selected as the highest specific work. In addition, Hu et al. (2020) evaluated an ORC that utilized R1234ze(E), R1234ze(Z), R1234yf, R134a, R1243zf, R600a, R245fa, R1234yd(Z), R1233zd(E), and R1336mzz(Z) as typical, famous, and low GWP organic refrigerant working fluids as well. This study conducted a numerical target preference and multi-criteria decision-making (MCDM) method. Overall, they found the R1234ze(E) was optimal and had the most considerable power output of 50.8 kW, which was 14% higher than R245fa. Zhai et al. (2016) analyzed the 30 different working fluids, including a new environmentally friendly it, R1234yf, by applying subcritical ORC for open-type heat sources with temperatures from 150 to 350 °C, water to air, respectively as heat sources. Their achievement illustrated that Cyclohexane had the highest exergy efficiency, and RC318 had the lowest. Manente et al. (2017), in terms of using subcritical working conditions besides the comparison between dual pressure and the single pressure layout in the ORC systems that utilized a heat source, geothermal 100-200 °C performed a simulation by EES (Engineering Equation Solver) on some new, low GWP and ODP environmental friendly and also new working fluids like; R1234yf, R1234ze(E), and R1234ze(Z) in parallel with some old, famous, and typical working fluids such as; R134a, iC4, R245fa, iC5, and cC5. Their achievements revealed that R1234ze(E) and R1234yf had the highest and optimum net power output, total cycle efficiency, and thermal efficiency compared with the other working fluids.

Many scholars try to consider, evaluate, and compare pure and zeotropic mixtures of working fluids that drive ORC and pay attention to the thermodynamic analysis. For instance, Zhai et al. (2018) paid attention to zeotropic mixtures and pure working fluids of various types of old and new environmental working fluids in ORC and focus analyzed the performance parameters. Based on this study, applied in subcritical working conditions, the highest optimum cycle exergy efficiency belonged to 0.3R1234ze(E)/0.7R245fa with 44.45% in a subcritical ORC using a 210 °C heat source. Regarding thermo-economic

parameters, R236ea, R227ea, R245fa, and 0.2R227ea/0.8R245fa had the lowest cost value of the application, and R1234ze(E) had the highest cost value of the present ORC application. Kang et al. (2015) analyzed ten groups of old and low GWP working fluids, including HCs, HFCs, and HFOs. Furthermore, by applying Matlab and Refprop as numerical simulation software, they investigated the performances of an ORC in terms of geothermal heat source (120 °C). In conclusion, the impact of different evaporation temperatures on net power output, exergy efficiency, and thermal efficiency depicted the R1234yf/R601a (0.7/0.3) had the maximum optimum value compared with other zeotropic mixtures of working fluids. Zheng et al. (2018) performed a solar ORC integrated with vapor compression cycle (VCC) driving by R290, R161, R152a, R134a, R600a, R227ea, R1234yf, and R1234ze as pure working fluids and R290/R600a, R152a/R600a, R161/R600a, R227ea/R600a, and R1234yf/R600a as binary zeotropic mixtures of working fluid to improve the overall system performance. In a nutshell, among their working fluids, R161/R600a (0.25/0.75) revealed the highest optimum system efficiency with 0.3089. Moreover, in comparison, with pure working fluids R161 and R600a, the total efficiency of their binary zeotropic mixture showed a 54.7% and 39.6% increase, respectively.

Most present scholars pay attention to modeling and performing the organic Rankine cycle base on complex and particular initial working conditions by applying the pure and finally the fixed binary zeotropic mixtures of working fluids with small scale power generate and low exergy efficiency in parallel to the high investment cost and payback period. In contrast, this study uses the subcritical organic Rankine cycle in a simple structure and driven by pure, fixed binary zeotropic mixtures and a fixed ternary zeotropic mixture of two green and environmental friendly refrigerant working fluids beside an old but famous working fluid, efforts to generate optimum and large-scale power that suitable for CPI (>1MW) by utilizing the flue gas as a heat source with medium temperature, open kind, and no restriction of the outlet temperature to increase the exergy efficiency and reduce the investment cost and payback period in optimum values.

In current scholar, designing, modeling, simulating, analyzing, and investigating the Subcritical Organic Rankine Cycle (SORC) under steady-state conditions and simple structure also driven by pure, fixed binary zeotropic mixtures and a fixed ternary zeotropic mixture of two environmentally friendly and new working fluids like R1234ze(E) and R1234yf and an old and famous organic refrigerant working fluid like R134a, based on applying the flue gas as a heat source with medium temperature, open kind, and no restriction of the outlet temperature of heat source in the evaporation process, also the flue gas is released from industrial boilers, and then try to improve the exergy and total efficiency parameters and parallel with SIC, PPC, and PBP as thermo-economic parameters cause to generating optimum net power output.

MATERIALS AND METHODS

The System of ORC and its Thermodynamic Process

Figure 1 shows that the Subcritical Organic Rankine Cycle (SORC) applies R1234ze(E), R1234yf, and R134a as pure working fluids, R1234ze(E)/R1234yf (0.5/0.5), R1234ze(E)/R134a (0.5/0.5), and R1234yf/R134a (0.5/0.5) as fixed binary zeotropic mixtures of working fluids, the R1234ze(E)/R1234yf/R134a (0.4/0.3/0.3) as a fixed ternary zeotropic mixture of working fluid and the current SORC system is including; a pump, an evaporator, a vapor generator, a turbine, and a condenser. Figures 1 and 2 depict the schematic diagram of the current SORC system and, in parallel, the T-S diagram of the SORC thermodynamic process. Furthermore, in Figures 1 and 2, the thermodynamic state points are shown the thermodynamic process of the present SORC system.

Figures 1 and 2 belong to the SORC system; first, under a subcritical state, the working fluid in the saturated liquid state by using a feed pump is pressurized to subcooled liquid (1–2 process) as a compression process. Then the working fluid in a high-pressure by using an evaporation process, including an evaporator and a vapor generator, absorbs heat by applying a heat

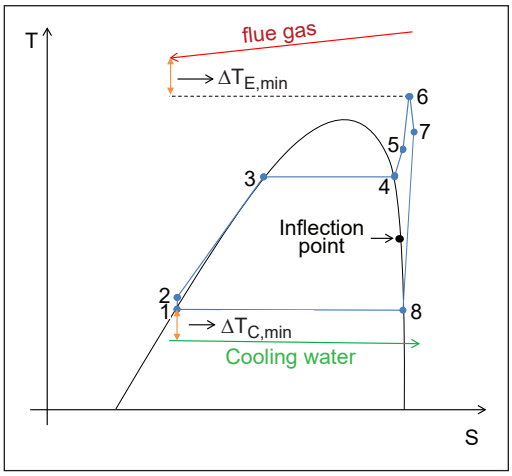

Figure 2. SORC thermodynamic process by applying flue gas as a heat source, cooling water as a heat sink, and using the Pure, Binary Zeotropic, and Ternary Zeotropic Mixtures of R1234ze(E), R1234yf, and R134a as Working Fluids

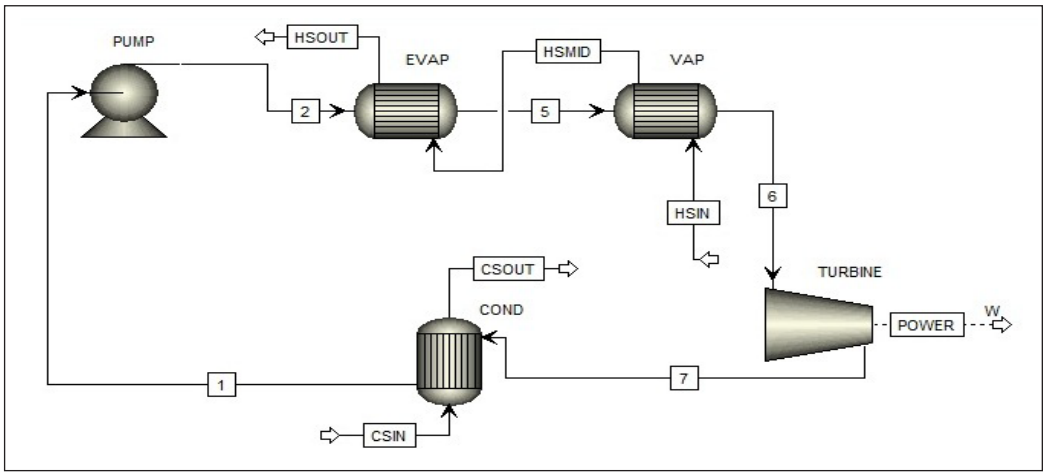

Figure 1. Schematic of the considered SORC system driven by pure, binary zeotropic, and ternary zeotropic mixtures of R1234ze(E), R1234yf, and R134a as Working Fluids

source, flue gas, and converts into saturated and then superheated vapor (2–3 process: preheating, 3–4 process: evaporation, 4–6 process: superheating). The vapor expands in the turbine and generates optimum power (6–7 process) as an expansion process. Finally, the working fluid discharges in a condenser and cools into saturated liquid (7–1 process) as a condensation process by contributing a heat sink and cooling water to complete this thermodynamic cycle.

Thermophysical Properties of Working Fluids

Table 1 presents the thermophysical properties of R1234ze(E), R1234yf, and R134a (Yang et al., 2020; Wang et al., 2020; Tian et al., 2020; Braimakis et al., 2020; Liu et al., 2020; Ata et al., 2020).

Table 1
Thermophysical properties of R1234ze(E), R1234yf, and R134a

Working Fluid	R1234ze(E)	R1234yf	R134a
Chemical Name	trans-1,3,3,3-tetrafluoroprop-1-ene	2,3,3,3-tetrafluoroprop-1-ene	1,1,1,2-tetrafluoroethane
Molecular Formula	CHF=CHCF3 (trans)	CF3CF=CH2	CF3CH2F
Normal Boiling Point at 101.3 kPa/ °C	-18.97	-29.48	-26.07
Critical Pressure/ MPa	3.635	3.382	4.059
Critical Temperature/℃	109.36	94.70	101.06
Molecular Weight/ g/mol	114.04	114.04	102.03
Appearance	Colorless	Colorless	Colorless
GWP	<1	<1	1300
ODP	0	0	0
Lifetime in the Atmosphere/days	~4900	10.5	16.4
Safety Classification	A2L	A2L	A1

R1234ze(E) and R1234yf are isentropic, but the type of R134a is wet. Besides, in the inflection point (S_{ip}), the entropy reaches the maximum value of the two-phase zone on the saturation vapor curve. Likewise, the saturation vapor curve slope is negative above this inflection point and $(^{dS}/_{dT})_{sat} < 0$, so the working fluid presents a wet property. On the other hand, the saturation vapor curve slope is positive below this inflection point and $(^{dS}/_{dT})_{sat} > 0$; therefore, the working fluid shows a dry-type property.

Model Boundary Condition of SORC system

Tables 2, 3, and 4 show a list of the boundary conditions and the constraints of the present SORC system. The flue gas is a heat source with medium temperature, open kind, and no restriction of the outlet temperature of heat source chosen in the evaporation process; also, this kind of flue gas is released from industrial boilers. The inlet temperature of flue gas as

the medium temperature fixed at 220 °C and 0.1013 MPa; moreover, the heat source outlet temperature can decrease to ambient temperature or $T_2+\Delta T_{e,min}$ without restriction. On the other hand, the superheated temperature was set to 5 °C increases to avoid the expansion process not passing through the two-phase region and based on the flash tolerance of each

Table 2
SORC system boundary conditions and constraints of pure working fluids

Parameter	Symbol	R1234ze(E)	R1234yf	R134a
Working Fluid mass flow rate/kg.s^{-1}	$\dot{m}_{wf}$	277.778	277.778	277.778
flue gas mass flow rate/kg.s^{-1}	$\dot{m}_{HS}$	555.556	555.556	555.556
Cooling water mass flow rate/kg.s^{-1}	$\dot{m}_{CS}$	555.556	555.556	555.556
Mole Fractions	-	1	1	1
flue gas pressure/kPa	P_{HS}	101.325	101.325	101.325
flue gas inlet temperature/°C	$T_{HS,in}$	220	220	220
Condenser minimal temperature difference/°C	$\Delta T_{cond,min}$	15.098	4.329	5.735
Evaporator minimal temperature difference/°C	$\Delta T_{evap,min}$	73.038	85.23	83.469
Cooling water pressure/kPa	P_{CS}	101.325	101.325	101.325
Cooling water inlet temperature/°C	$T_{CS,in}$	10	10	10
Environment pressure/kPa	P_0	101.325	101.325	101.325
Environment temperature/°C	T_0	20	20	20
Feed pump efficiency/%	η_p	85	85	85
Feed pump pressure head/m	H	105.236	108.335	98.621
Turbine efficiency/%	η_t	72	72	72

Table 3
SORC System boundary conditions and constraints of binary zeotropic working fluids

Parameter	Symbol	R1234ze(E)/ R1234yf	R1234ze(E)/ R134a	R1234yf/ R134a
Working Fluid mass flow rate/kg.s^{-1}	$\dot{m}_{wf}$	277.778	277.778	277.778
flue gas mass flow rate/kg.s^{-1}	$\dot{m}_{HS}$	555.556	555.556	555.556
Cooling water mass flow rate/kg.s^{-1}	$\dot{m}_{CS}$	555.556	555.556	555.556
Mole Fractions	-	0.5/0.5	0.5/0.5	0.5/0.5
flue gas pressure/kPa	P_{HS}	101.325	101.325	101.325
flue gas inlet temperature/°C	$T_{HS,in}$	220	220	220
Condenser minimal temperature difference/°C	$\Delta T_{cond,min}$	8.538	7.325	4.982
Evaporator minimal temperature difference/°C	$\Delta T_{evap,min}$	79.844	81.433	84.516
Cooling water pressure/kPa	P_{CS}	101.325	101.325	101.325
Cooling water inlet temperature/°C	$T_{CS,in}$	10	10	10
Environment pressure/kPa	P_0	101.325	101.325	101.325
Environment temperature/°C	T_0	20	20	20
Feed pump efficiency/%	η_p	85	85	85
Feed pump pressure head/m	H	106.697	102.126	103.675
Turbine efficiency/%	η_t	72	72	72

Table 4
SORC system boundary conditions and constraints of ternary zeotropic working fluids

Parameter	Symbol	R1234ze(E)/R1234yf/R134a
Working Fluid mass flow rate/kg.s^{-1}	$\dot{m}_{wf}$	277.778
flue gas mass flow rate/kg.s^{-1}	$\dot{m}_{HS}$	555.556
Cooling water mass flow rate/kg.s^{-1}	$\dot{m}_{CS}$	555.556
Mole Fractions	-	0.4/0.3/0.3
flue gas pressure/kPa	P_{HS}	101.325
flue gas inlet temperature/°C	$T_{HS,in}$	220
Condenser minimal temperature difference/°C	$\Delta T_{cond,min}$	7.0725
Evaporator minimal temperature difference/°C	$\Delta T_{evap,min}$	81.805
Cooling water pressure/kPa	P_{CS}	101.325
Cooling water inlet temperature/°C	$T_{CS,in}$	10
Environment pressure/kPa	P_0	101.325
Environment temperature/°C	T_0	20
Feed pump efficiency/%	η_p	85
Feed pump pressure head/m	H	104.33
Turbine efficiency/%	η_t	72

working fluid in the evaporator. Likewise, each working fluid's mass flow rate is set to 277.778 kg.s^{-1}, and the mass flow rate of flue gas and cooling water is set to 555.556 kg.s^{-1} as the main effective parameters in parallel expansion enthalpy change on the optimum power generating. There are some constraints of this study as well.

The lower and upper limits of P_2 (compression pressure) based on subcritical working conditions investigate because these limit values are accessible, efficient, relatively safe, and economical to achieve. Furthermore, to prevent the influence of the significant thermophysical property variations close to the critical zone of each working fluid. The optimized variable input parameter is compression pressure. Also, it defines as a turbine inlet pressure. In the cycle, the pump's inlet pressure lower limit increase sets into the 0.4 MPa (reach into the 1.4 MPa as a minimum boundary condition of compression pressure) to mitigate air ingress and prevent sub-atmospheric pressure leading to approach optimum net power output generated (>1MW). Moreover, the upper limit of compression pressure increase is set to 1.2 MPa (reach into the 2.2 MPa as a maximum boundary condition of compression pressure) to prevent the flash calculation failed, and temperature cross detected in the T-Q diagram of the evaporator.

Assumptions

The following general assumptions are made to simplify the current SORC system analysis:

- Simplifying the complexity of the model.
- Steady-state operating of the SORC system.
- Neglecting heat and pressure loss in heat exchangers and pipes.

- Friction pressure drop is neglected in pipelines and heat exchangers.
- Neglecting the influence of gravitational potential energy and fluid kinetic.
- The heat exchangers arrangement in a countercurrent flow type.
- Supplying the constant temperatures for the evaporation system's heat source and the condenser's heat sink.

The SORC System Theoretical Equations

The Thermodynamic Equations. The net power output generated by the SORC system is as in Equation 1:

$$W_{net}=W_T-W_P \quad [1]$$

Where W_t is the turbine power generated, W_P is the pump power consumed.

The heat absorption capacity of the SORC system is as in Equation 2:

$$Q_{SORC}=\dot{m}_{HS}\left(h_{HS,in}-h_{HS,out}\right) \quad [2]$$

Where $\dot{m}_{HS}$ is the flue gas mass flow rate, also $h_{HS,in}$ and $h_{HS,out}$ are the flue gas inlet and outlet enthalpies, respectively.

The SORC total efficiency is as in Equation 3:

$$\eta_{SORC}=\frac{W_{net}}{Q_{SORC}} \quad [3]$$

The T_0=20 °C and P_0=101.325 kPa are chosen as the environment state reference. The exergy released in the evaporator and vapor generator system by the heat source is as in Equation 4:

$$\Delta E_{HS}=\dot{m}_{HS}(h_{HS,in}-h_{HS,out}-T_0(S_{HS,in}-S_{HS,out})) \quad [4]$$

Where $S_{HS,in}$ and $S_{HS,out}$ are the inlet and outlet of the heat source entropies, respectively. The exergy absorbed in the evaporator and vapor generator system by the working fluid is as in Equation 5:

$$\Delta E_{wf,abs}=\dot{m}_{wf}(h_6-h_2-T_0(S_6-S_2)) \quad [5]$$

Where $\dot{m}_{wf}$ is the working fluid mass flow rate, likewise h_6 and h_2 are the vapor generator outlet enthalpy and the evaporator inlet enthalpy, respectively. Moreover, S_6 and S_2 are the vapor generator outlet entropy and the evaporator inlet entropy, respectively.

Hence, the evaporator and vapor generator exergy destruction rates (the exergy loss or the unused exergy) of application are as in Equation 6:

$$I_{E,V}=\Delta E_{HS}-\Delta E_{wf,abs}=T_0(\dot{m}_{wf}(S_6-S_2)-\dot{m}_{HS}\left(S_{HS,in}-S_{HS,out}\right)) \quad [6]$$

The turbine exergy destruction rate is as in Equation 7:

$$I_T=T_0\dot{m}_{wf}(S_7-S_{7s}) \quad [7]$$

Where S_7 and S_{7s} are the turbine outlet and isentropic state entropies, respectively.
The pump exergy destruction rate is as in Equation 8:

$$I_P=T_0\dot{m}_{wf}(S_2-S_{2s}) \quad [8]$$

Where S_2 and S_{2s} are the pump outlet and isentropic state entropies, respectively.
Similar to the evaporator and vapor generator system heat transfer process, the condenser exergy release is as in Equation 9:

$$\Delta E_{wf,rel}=\dot{m}_{wf}(h_7-h_1-T_0(S_7-S_1)) \quad [9]$$

Where h_1 and h_7 are the condenser outlet and inlet enthalpies, respectively. Moreover, S_1 and S_7 are the condenser outlet and inlet entropies, respectively.
Also, the exergy absorbed from the condenser by the heat sink is as in Equation 10:

$$\Delta E_{CS}=\dot{m}_{CS}(h_{CS,out}-h_{CS,in}-T_0(S_{CS,out}-S_{CS,in})) \quad [10]$$

Where $\dot{m}_{CS}$ is the cold stream as a heat sink mass flow, moreover $h_{CS,out}$ also $h_{CS,in}$ are the cold stream outlet and inlet enthalpies, respectively. Furthermore, $S_{CS,out}$ and $S_{CS,in}$ are the cold stream outlet and inlet entropies, respectively.
So, the condenser exergy destruction rate is as in Equation 11:

$$I_C=\Delta E_{wf,rel}-\Delta E_{CS}=T_0(\dot{m}_{CS}(S_{CS,out}-S_{CS,in})-\dot{m}_{wf}(S_7-S_1)) \quad [11]$$

The exergy balance of the SORC system is declared by Equation 12:

$$\Delta E_{HS}+\Delta E_{CS}=W_t-W_P+\sum I_i \quad [12]$$

In each process of the present SORC system, the exergy destruction rate coefficient is as in Equation 13:

$$\xi_i=\frac{I_i}{\Delta E_{HS}-\Delta E_{CS}} \quad [13]$$

To sum up, the exergy destruction rate coefficient of the SORC system rate is given by Equation 14:

$$\xi_{SORC}=\sum \xi_i=\frac{I_{E,V}+I_T+I_P+I_C}{\Delta E_{HS}-\Delta E_{CS}}=1-\frac{W_t-W_p}{\Delta E_{HS}-\Delta E_{CS}}=1-\frac{W_{net}}{\Delta E_{HS}-\Delta E_{CS}} \quad [14]$$

All in all, the total exergy efficiency is as in Equation 15:

$$\eta_{ex}=\frac{W_{net}}{\Delta E_{HS}-\Delta E_{CS}}=1-\sum \xi_i \quad [15]$$

The Thermo-Economic Equations of the SORC System

Evaluation of the thermo-economic parameters as a substitute for the efficiency of the SORC system consists of specific investment cost (SIC), power production cost (PPC), and payback period (PBP).

The cost of all components of the current SORC system is calculated using Equation 16:

$$Cost_{2001}=C_{bmE}+C_{bmV}+C_{bmC}+C_{bmT}+C_{bmP} \quad [16]$$

Where C_{bm} is the cost of SORC components and $Cost_{2001}$ is the cost of all components in 2001 presented by the chemical engineering plant cost index (CEPCI) (Turton et al., 2012).

Furthermore, converting the cost of all components from 2001 to 2021 can be achieved by using Equation 17:

$$Cost_{2021}=\frac{Cost_{2001}CEPCI_{2021}}{CEPCI_{2001}} \quad [17]$$

Which $CEPCI_{2001}$=397, $CEPCI_{2021}$=624.0269 (Turton et al., 2012; Mignard, 2014).

Hence, the cost of SORC components is given by Equations 18-29:

For evaporator:

$$\log C_{pE}=K_1+K_2\log(A_E)+K_3[\log(A_E)]^2 \quad [18]$$

$$C_{bmE}=C_{pE}F_{bmE} \quad [19]$$

For vapor generator:

$$\log C_{pV}=K_1+K_2\log(A_V)+K_3[\log(A_V)]^2 \quad [20]$$

$$C_{bmV}=C_{pV}F_{bmV} \quad [21]$$

For condenser:

$$\log C_{pC}=K_1+K_2\log(A_C)+K_3[\log(A_C)]^2 \quad [22]$$

$$C_{bmC}=C_{pC}F_{bmC} \quad [23]$$

For pump:

$$\log C_{pP}=K_1+K_2\log(W_P)+K_3[\log(W_P)]^2 \quad [24]$$

$$\log F_{pP} = C_1 + C_2 \log (W_P) + C_3 [\log (W_P)]^2 \quad [25]$$

$$F_{bmP} = B_1 + B_2 F_M F_{pP} \quad [26]$$

$$C_{bmP} = C_{pP} F_{bmP} \quad [27]$$

For turbine:

$$\log C_{pT} = K_1 + K_2 \log (W_T) + K_3 [\log (W_T)]^2 \quad [28]$$

$$C_{bmT} = C_{pT} F_{bmT} \quad [29]$$

Where the K_1, K_2, K_3, C_1, C_2, C_3, B_1, B_2, F_{bm} , F_M are the cost price correction factors of evaporator "E", vapor generator "V", condenser "C", pump "P", and turbine "T", as displayed in Table 5.

Table 5
Correlation coefficient of SORC components cost (Turton et al., 2012)

	K_1	K_2	K_3	C_1	C_2	C_3	B_1	B_2	F_M	F_{bm}
Evaporator, Vapor Generator, and Condenser	4.6420	0.3698	0.0025	/	/	/	/	/	/	2.9
Pump	3.3892	0.0536	0.1538	0	0	0	1.89	1.35	1.5	/
Turbine	2.7051	1.4398	0.1776	/	/	/	/	/	/	3.5

Besides, the cost of labor is calculated using Equation 30:

$$Cost_{Labor} = 0.3 Cost_{2021} \quad [30]$$

In a nutshell, one of the foremost performance parameters which equivalent to the profitability of the SORC system is the specific investment cost (SIC) that, based on neglecting the maintenance and insurance annual cost, is calculated using Equation 31:

$$SIC = \frac{Cost_{2021} + Cost_{Labor}}{W_{net}} \quad [31]$$

Likewise, the heat source of the SORC system, flue gas, is assumed to be cost-free.

The capital recovery factor (CRF) is a prerequisite factor of power production cost (PPC) and as a converter parameter to convert a current value into an annual cost base on a specified time and discount rate is calculated using Equation 32:

$$CRF = \frac{i(1+i)^{LT}}{[(1+i)^{LT} - 1]} \quad [32]$$

Where i is the annual interest rate and assumed to be 5%, LT is the system lifetime and assumed to be 15 years.

The cost of the SORC system to generate the net power output is power production cost (PPC) and achieved by using Equation 33:

$$PPC=\frac{[CRFCost_{2021}+iCost_{2021}]}{(W_{net}t_{op})} \quad [33]$$

Where t_{op} is the system operation time and assumed to be 7500 h annually (Nafey & Sharaf, 2010).

The payback period (PBP) is the period that is needed to recover the total investment cost of the SORC system and is calculated using Equation 34:

$$PBP=\frac{\ln[(W_{net}C_e)/(iCost_{2021}-W_{net}C_e)]}{\ln(1+i)} \quad [34]$$

Where C_e is the power price in 2021 in the U.S. and assumed to be 0.0696 $/kWh (https://www.eia.gov/outlooks/steo/report/electricity.php).

RESULT AND DISCUSSION

Simulation Software Validation

The validity confirmation of SORC system components, R1234ze(E), R1234yf, and R134a as working fluids, heat source (flue gas), heat sink (cold water) in the AspenPlus (v10) simulation software has been valid extensively. Most current results in this study have been validated and tested using established data and compared with several results in a similar condition from published works of literature as having been done, accepted, and published in the past. The current results from the AspenPlus (v10) are consistent, with no significant deviation arising for all trials.

The AspenPlus (v10) software's library source comprehensively uses several equations of state as a calculation method to evaluate and estimate the number of thermodynamic parameters in the SORC system. Hence, based on the current SORC system condition for more accuracy, the REFPROP selects as an equation of state in this simulation. In the present study, the significant number of results before this is done and published by other scholars with similar conditions compared and verified by the current results of this study. The proposed SORC system is a novel configuration and has not been studied and considered in previous literature. So, to verify and validate the current study conducted in the same condition in Li et al. (2017). As shown in Table 6, the total efficiency and net power output of R1234ze(E) in the present SORC system investigate by comparison with Li et al. (2017), with the maximum derivation from the date in reference is 10.00% for the

total efficiency of the SORC system. Since each section's derivation of this SORC system is reasonably negligible, the simulation model and the results were accurate enough for further investigations.

Table 6
Verification and validation of the simulation results of the present work with Li et al. (2017)

P_T (MPa)	T_T (°C)	$\eta_{Present}$ (%)	$\eta_{Ref.}$ (%)	%	$W_{net,Present}$ (kW)	$W_{net,Ref.}$ (kW)	%
1.58	109.144	0.064	0.071	9.86	44.12	44.80	1.52
1.38	103.285	0.057	0.062	8.06	38.47	39.00	1.36
1.18	96.748	0.048	0.051	5.88	31.77	33.00	3.73
0.98	89.318	0.036	0.040	10.00	23.64	24.80	4.68

Performance Analysis of Subcritical Organic Rankine Cycle (SORC)

Figure 3 illustrates the effect of different compression pressure (1.4–2.2 MPa) on the net power output of R1234ze(E), R1234yf, and R134a as pure working fluids, R1234ze(E)/R1234yf (0.5/0.5), R1234ze(E)/R134a (0.5/0.5), and R1234yf/R134a (0.5/0.5) as fixed binary zeotropic mixtures of working fluids, and the R1234ze(E)/R1234yf/R134a (0.4/0.3/0.3) as a fixed ternary zeotropic mixture of working fluid. As a result, the highest

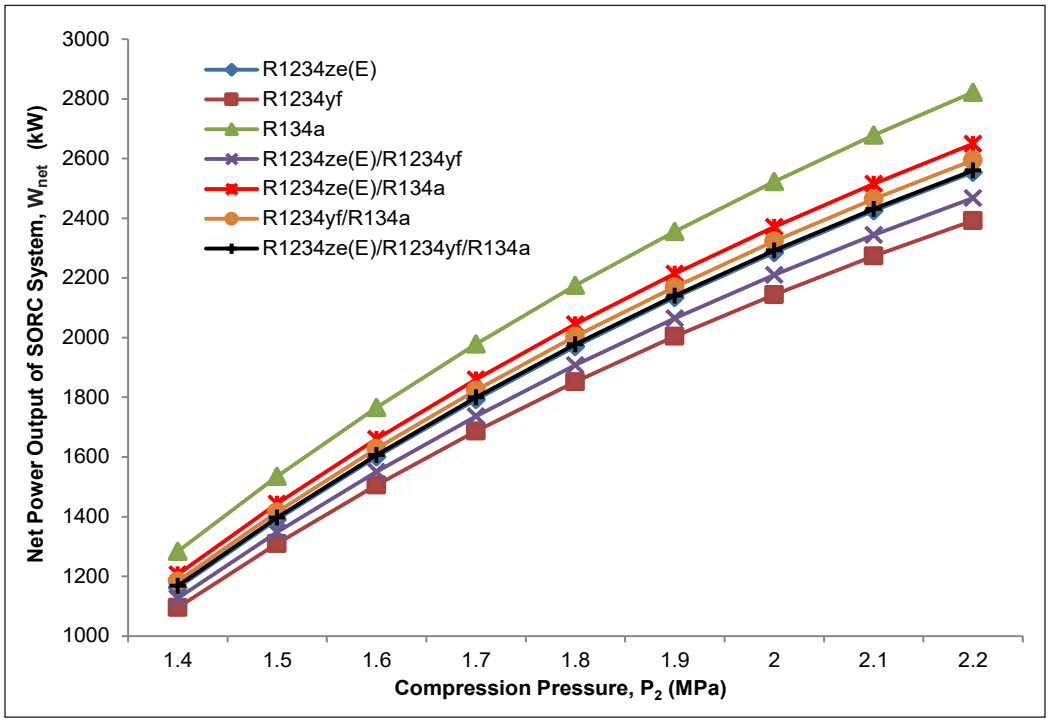

Figure 3. The net power output generated by SORC system at different compression pressures of R1234ze(E), R1234yf, R134a, R1234ze(E)/R1234yf, R1234ze(E)/R134a, R1234yf/R134a, and R1234ze(E)/R1234yf/R134a as working fluids

SORC net power output range is 1283.22 KW to 2822.04 KW and belongs to the R134a. Also, the lowest range of net power output corresponding to R1234yf with 14.62–15.24% reduction shows 1095.58 KW to 2391.81 KW. Therefore, between the highest to the lowest range of SORC system net power output, the R1234ze(E)/R134a with 1207.02–2650.02 KW, R1234yf/R134a with 1183.86-2595.13 KW, R1234ze(E)/R1234yf/R134a with 1167.92–2560.27 KW, R1234ze(E) with 1162.40–2554.04 KW, and R1234ze(E)/R1234yf with 1127.27–2467.84 KW are adapted, respectively. As depicted in Figure 3, increasing the compression pressure causes an increase in the evaporation temperature as a consequence of enthalpy change of flue gas and the evaporation process growth, and totally the conclusion increases the turbine output power and, as a result, increases the net power output in each working fluid. The main reason for these fluctuations between different kinds of working fluids is that the increasing expansion enthalpy change of each working fluid leads to an increase in the net power output because of the turbine enthalpy conversion into power. In parallel, the flue gas enthalpy changes in the evaporation system and, therefore, the heat absorption capacity reveals to a large extent the positive relationship with the SORC system net power output. These results agree with Invernizzi et al. (2016) and Bianchi et al. (2020).

As depicted in Figure 4, the impact of different compression pressure (1.4-2.2 MPa) considered on the heat absorption capacity of R1234ze(E), R1234yf, and R134a as pure working fluids, R1234ze(E)/R1234yf (0.5/0.5), R1234ze(E)/R134a (0.5/0.5), and R1234yf/

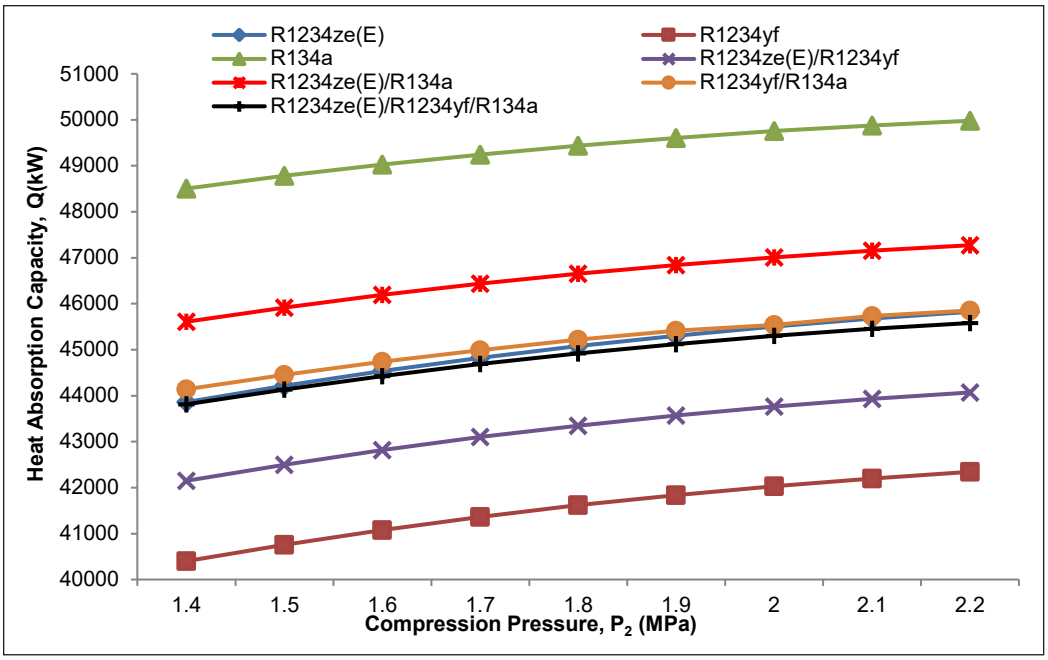

Figure 4. The heat absorption capacity of SORC system at different compression pressures of R1234ze(E), R1234yf, R134a, R1234ze(E)/R1234yf, R1234ze(E)/R134a, R1234yf/R134a, and R1234ze(E)/R1234yf/R134a as working fluids

R134a (0.5/0.5) as fixed binary zeotropic mixtures of working fluids, and the R1234ze(E)/R1234yf/R134a (0.4/0.3/0.3) as a fixed ternary zeotropic mixture of working fluid. The quantitative amount of heat absorption capacity of SORC belongs to the R134a as the highest amount with the value range of 48505.59–49983.37 kW, and the lowest amount belongs to the R1234yf, with a 16.71–15.28% reduction for the minimum to maximum compression pressure, as well. Likewise, the R1234ze(E)/R134a, R1234yf/R134a, R1234ze(E), R1234ze(E)/R1234yf/R134a, and R1234ze(E)/R1234yf are placed between highest amount to lowest amount of heat absorption capacity, respectively. By analyzing and investigating the heat absorption capacity as the main parameter of energy recovery and its equation, the flue gas enthalpy change significantly affects the heat absorption capacity of the SORC system. This parameter is directly related to the mass enthalpy change in the evaporation and, therefore, in the expansion process of each working fluid as a most effective parameter to generate optimum turbine power output. To sum up, these results similar to the results of Ji et al. (2021), Rowshanaie et al. (2020), and Rowshanaie et al. (2015).

As illustrated in Figure 5, the simulation model of SORC overall efficiency using Matlab Simulink software in Equations 1, 2, and 3 are considered and calculated to enhance the analysis accuracy in the current study.

From Figure 6, the total efficiency of SORC system for different compression pressures (1.4-2.2 MPa) of R1234ze(E), R1234yf, R134a, R1234ze(E)/R1234yf, R1234ze(E)/R134a, R1234yf/R134a, and R1234ze(E)/R1234yf/R134a as working fluids are disputed. Figure 6 indicates that the total efficiency of SORC has a positive relationship with compression pressure and, as a result, with the inlet pressure of the turbine. In parallel, the significant power generated by the turbine, minimal impact of power consumption by the pump, and the present SORC heat absorption capacity is the foremost reason for different insignificant values of total efficiency between each pure, binary zeotropic. Ternary zeotropic working

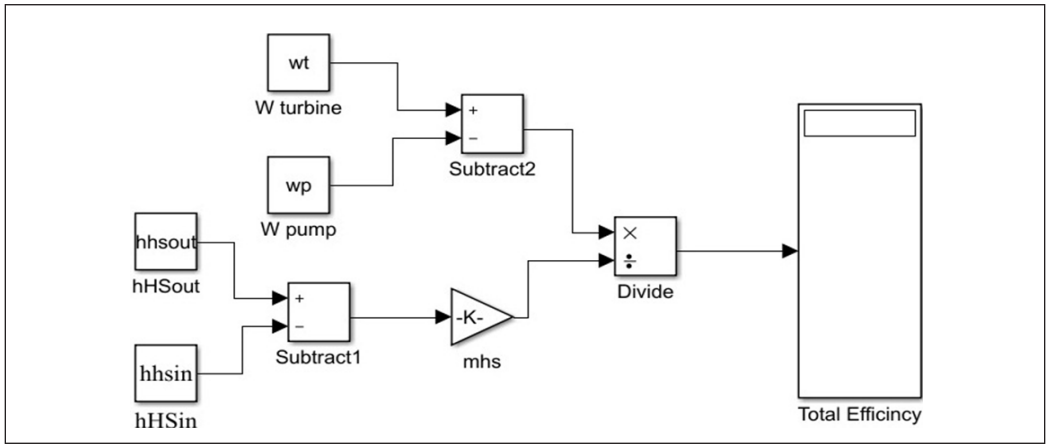

Figure 5. The total efficiency simulation analysis model of the SORC system

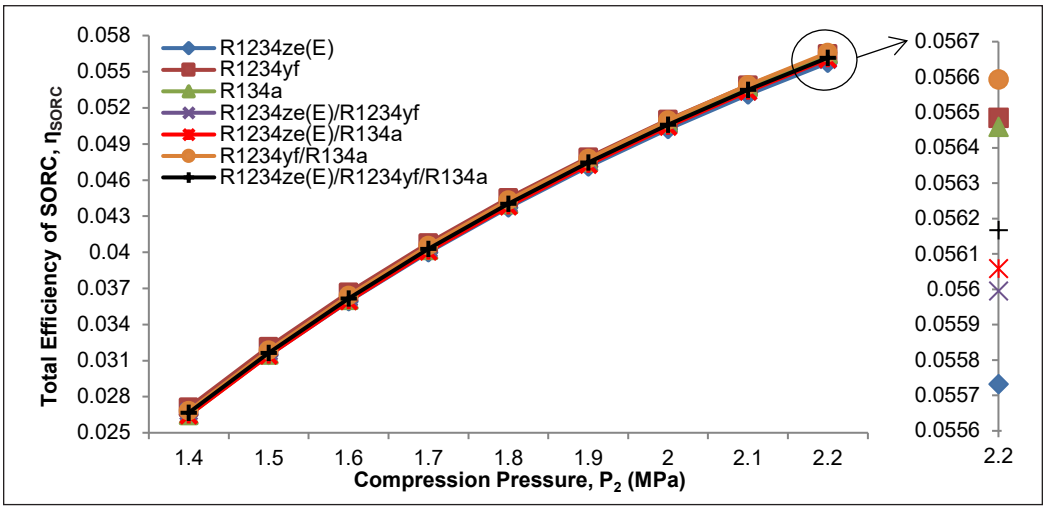

Figure 6. The total efficiency of SORC system at different compression pressures of R1234ze(E), R1234yf, R134a, R1234ze(E)/R1234yf, R1234ze(E)/R134a, R1234yf/R134a, and R1234ze(E)/R1234yf/R134a as working fluids.

fluids in each point of compression pressure or inlet pressure of turbine are minimum temperature differences at evaporation process, which has a direct relationship with a SORC overall efficiency. In brief, these results are similar to the results of Li et al. (2017), Vera et al. (2020), Cambi et al. (2016), and Rowshanaie et al. (2020).

Figure 7 shows the simulation model of exergy efficiency that calculates in the Matlab Simulink software by contributing Equations 1, 4, 10, and 15.

Figure 8 tries to indicate the influence of different compression pressures on the exergy efficiency of SORC for pure working fluids like; R1234ze(E), R1234yf, R134a, and binary zeotropic working fluids such as R1234ze(E)/R1234yf (0.5/0.5), R1234ze(E)/R134a (0.5/0.5), R1234yf/R134a (0.5/0.5), and ternary zeotropic working fluid including; R1234ze(E)/R1234yf/R134a. As illustrated in Figure 7, at the minimum boundary condition of compression pressure (1.4 MPa), the increasing trend of exergy efficiency starts from R1234ze(E)/R134a with 0.4866, R1234ze(E)/R1234yf with 0.4871, R134a with 0.4898, R1234yf/R134a with 0.4908, R1234ze(E) with 0.4946, R1234ze(E)/R1234yf/R134a with 0.4962 and reach to R1234yf with 0.5019 as the highest exergy efficiency in the lowest compression pressure of current SORC system. Hence, with increasing the compression pressure (1.4-2.2 MPa), the exergy efficiency of each working fluid grows dramatically. In this condition, at the maximum boundary condition of compression pressure (2.2 MPa), the increasing trend of exergy efficiency is started from R1234ze(E)/R1234yf/R134a with 0.6835, R1234ze(E)/R134a with 0.6855, R1234ze(E) with 0.6866, R1234yf with 0.6872, R1234ze(E)/R1234yf with 0.6881, R134a with 0.6905, and achieve to R1234yf/R134a with 0.6929 as the highest exergy efficiency in the highest compression pressure of present SORC system. The main impacts of these minimal differences between these pure, binary,

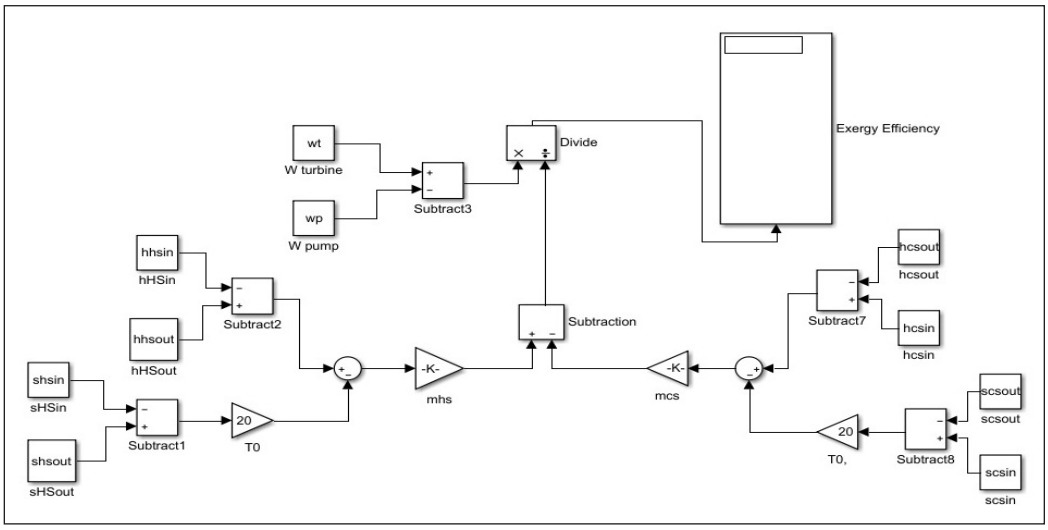

Figure 7. The exergy efficiency simulation analysis model of the SORC system

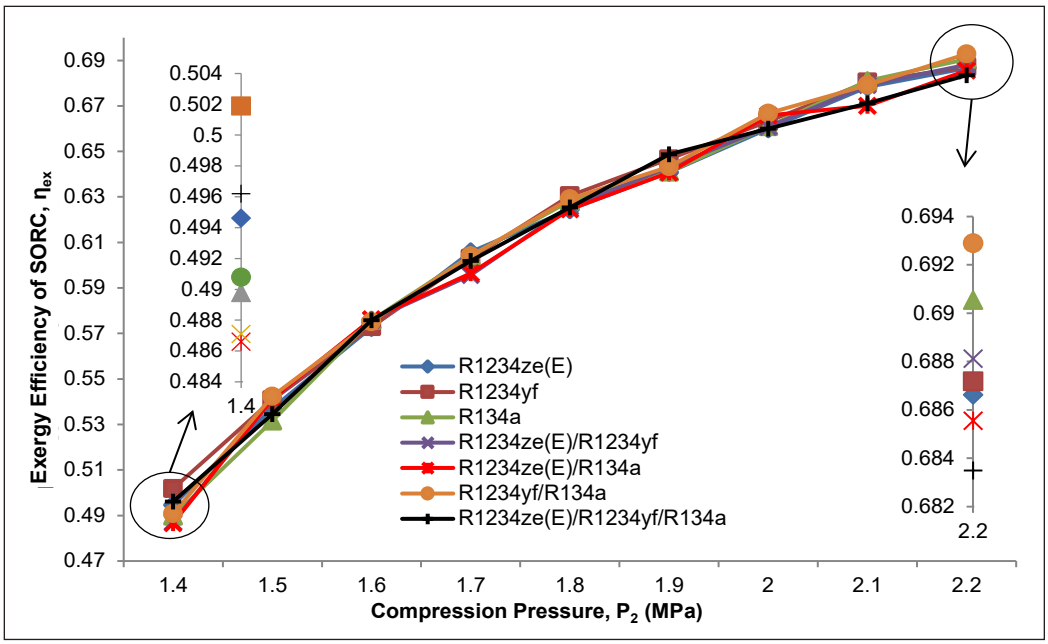

Figure 8. The SORC exergy efficiency at different compression pressures of R1234ze(E), R1234yf, R134a, R1234ze(E)/R1234yf, R1234ze(E)/R134a, R1234yf/R134a, and R1234ze(E)/R1234yf/R134a as working fluids

and ternary zeotropic working fluids are differences in power generated by the turbine and power consumed by the pump as a direct relationship with exergy efficiency. Also, in parallel, the flue gas and the cold water enthalpy different and entropy different have a direct relationship with exergy efficiency. Overall, these results are supported by Guo et al. (2021), Shengjun et al. (2011), and Rowshanaie et al. (2020).

The simulation calculation model of specific investment cost (SIC) as an essential economic efficiency parameter by Simulink of Matlab simulation software depicts in Figure 9, based on Equations 1 and 16-31.

Figure 10 compares the influence of different compression pressure (1.4–2.2 MPa) on specific investment cost (SIC) as economic efficiency of the current SORC system. As illustrated in Figure 10, increasing the compression pressure and enhancing the turbine inlet pressure will drastically glide the SIC. The maximum value to minimum value of SIC in terms of different compression pressure belongs to R134a with 5807402.18–22455670.61 $.kW^{-1}, and compared with this, the R1234ze(E)/R134a with 7.12–7.32% reduction, R1234yf/R134a with 9.11–9.42% reduction, R1234ze(E)/R1234yf/R134a with 10.52–10.88% reduction, R1234ze(E) with 10.99-10.95% reduction, R1234ze(E)/R1234yf with 14.12–14.46% reduction, and reach to the R1234yf with 16.82–17.38% reduction and achieve to the amount of 4830207.61–18551143.42 $.kW^{-1} as a minimum value of SIC. The foremost reasons are to increase the required exchanger area and, in parallel, to increase the net power generated by the turbine, leading to increasing cost of each component, including the pump, evaporator, vapor generator, turbine, and condenser; as a result cause to increasing SIC of SORC system, dramatically. It notes that these achievements are similar to Quoilin et al. (2011).

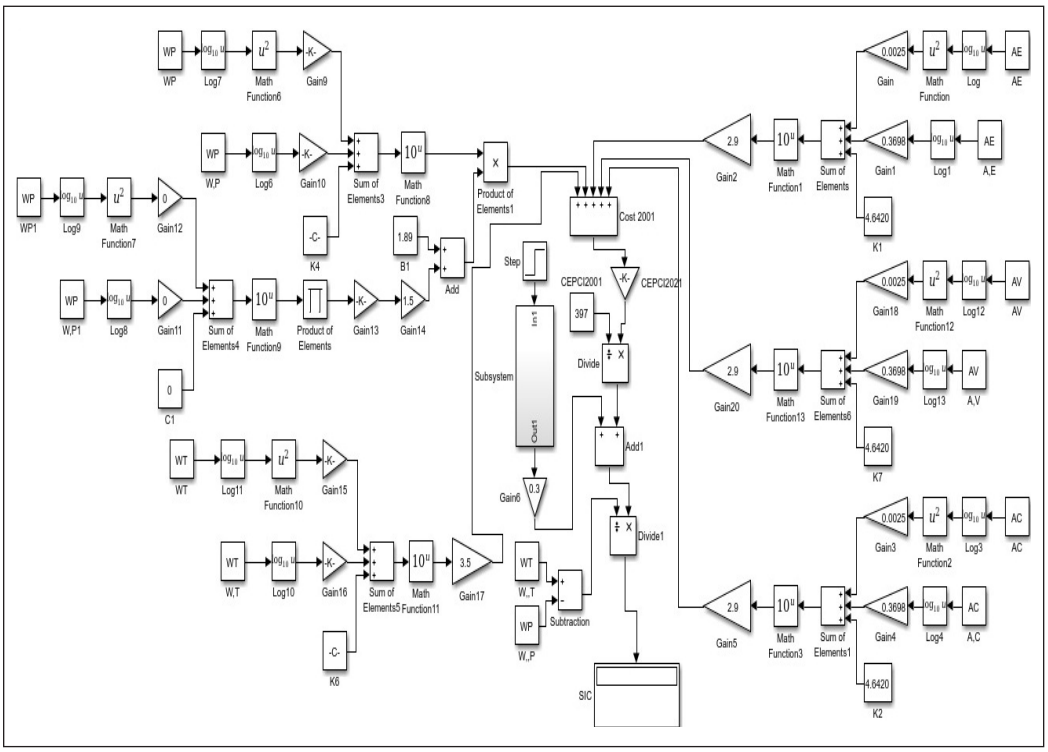

Figure 9. The SIC simulation analysis model of the SORC system

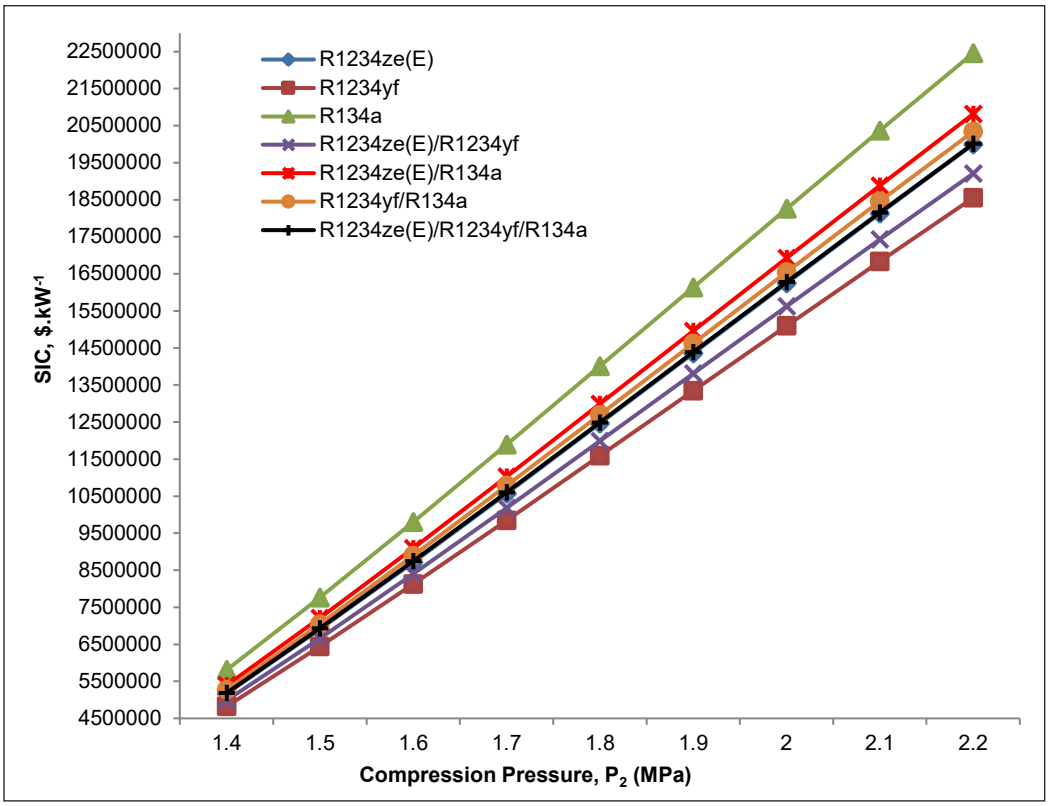

Figure 10. The specific investment cost (SIC) of SORC system at different compression pressures of R1234ze(E), R1234yf, R134a, R1234ze(E)/R1234yf, R1234ze(E)/R134a, R1234yf/R134a, and R1234ze(E)/R1234yf/R134a as working fluids

Figure 11 illustrates the calculation model of power production cost (PPC) in the Simulink of Matlab simulation software in Equations 1, 16–29, 32, and 33.

As considered in Figure 12, the relationship between the compression pressures and, in the same meaning, the turbine inlet pressure (1.4-2.2 MPa) and the power production cost (PPC) of the SORC system are discussed. As illustrated in this graph, the trend of PPC with increasing compression pressure depicts a positive correlation. In this condition, increasing the total cost of the present SORC application and the SORC system net power output at the same time is affected by flue gas enthalpy change, leading to increased PPC, remarkably. In Figure 12, the maximum to minimum range amount of PPC to comparison between different pure, binary, and ternary zeotropic working fluids belongs the R134a, R1234ze(E)/R134a, R1234yf/R134a, R1234ze(E)/R1234yf/R134a, R1234ze(E), R1234ze(E)/R1234yf, and R1234yf with values range of 81.74–316.07, 75.91–292.94, 74.29–286.30, 73.08–281.67, 72.76–281.44, 70.20–270.37, and 67.99–261.11 $.kW^{-1}.year^{-1}, respectively. The result of this economic parameter agrees with Li et al. (2019) and Zhang et al. (2017).

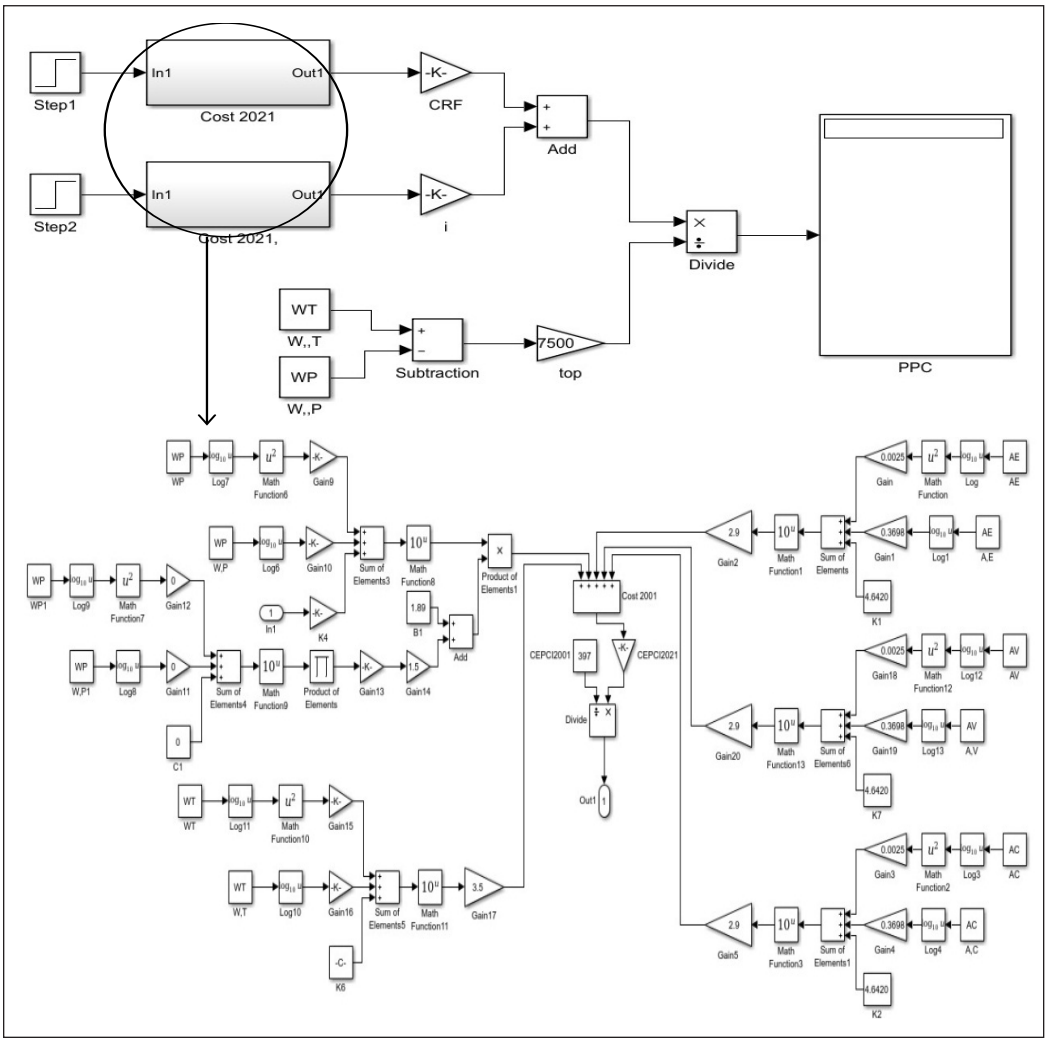

Figure 11. The PPC simulation analysis model of the SORC system

Figure 13 illustrates the simulation analysis method by applying the Simulink of Matlab simulation software for the payback period (PBP) of the SORC system by utilizing Equations 1 and 16–29.

The payback period (PBP) of the SORC system investigates different compression pressure; likewise, turbine inlet pressure (1.4–2.2 MPa) for each pure, binary, and ternary zeotropic working fluid is well present in Figure 14. As shown in this graph, the PBP of the current SORC system has a positive relationship with compression pressure and in parallel with turbine inlet pressure. Moreover, some essential thermodynamic parameters have a pivotal influence on enhancing the PBP in general. The main reasons for these fluctuation differences between each type of working fluids are the required exchanger's area, net power output, cost of each component, and heat absorption capacity. The lowest

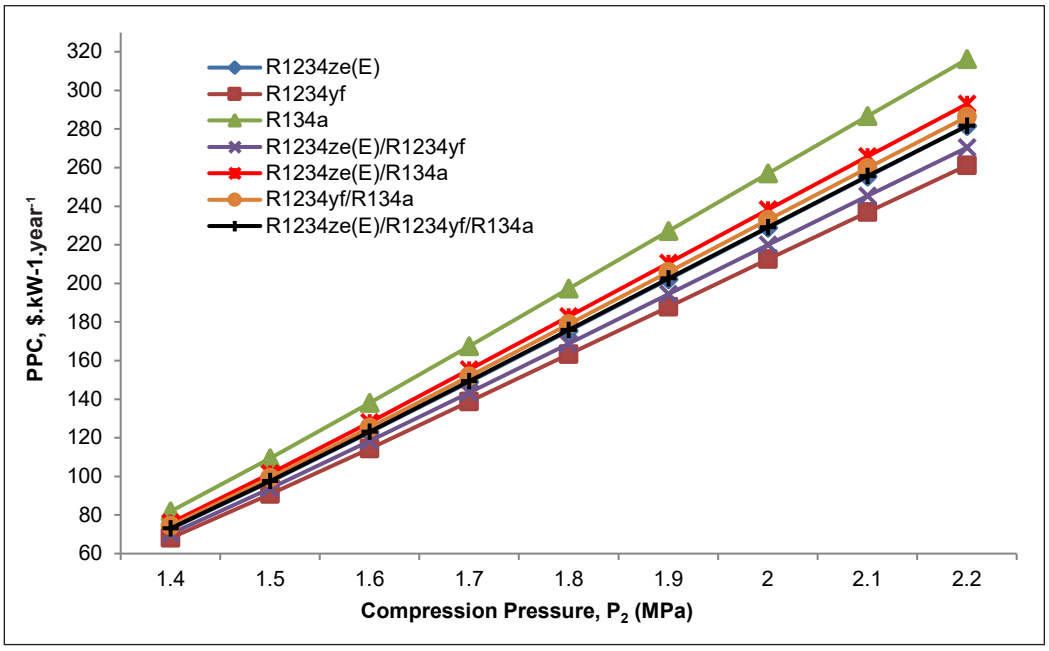

Figure 12. The power production cost (PPC) of SORC system at different compression pressures of R1234ze(E), R1234yf, R134a, R1234ze(E)/R1234yf, R1234ze(E)/R134a, R1234yf/R134a, and R1234ze(E)/R1234yf/R134a as working fluids

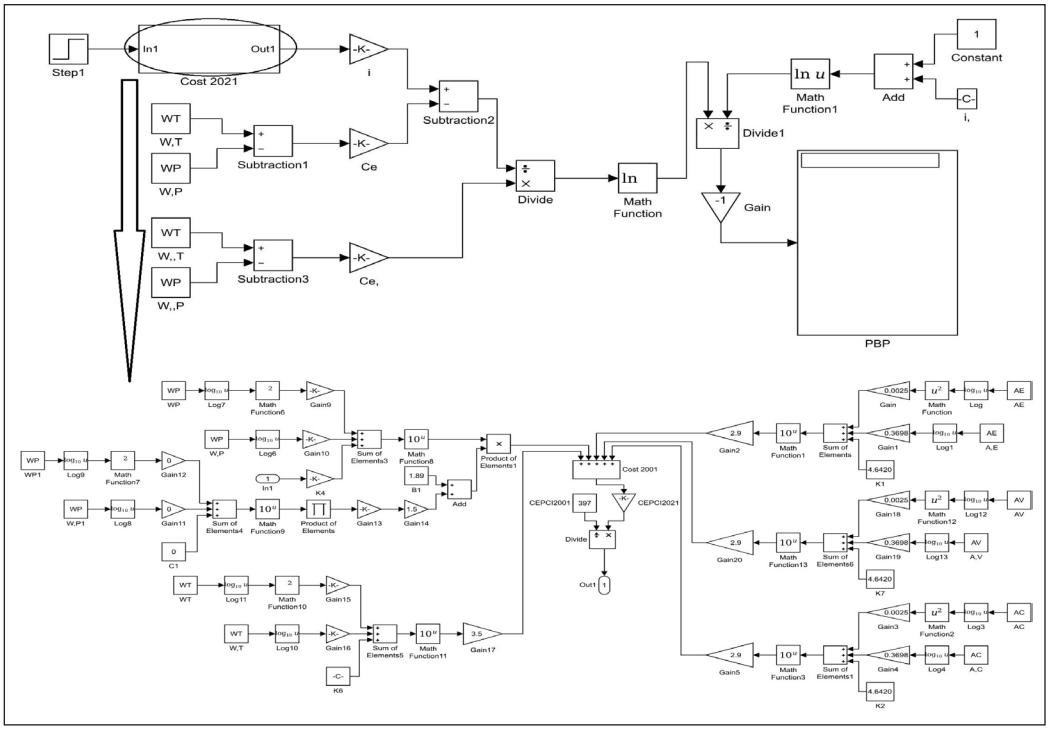

Figure 13. The PBP simulation analysis model of the SORC system

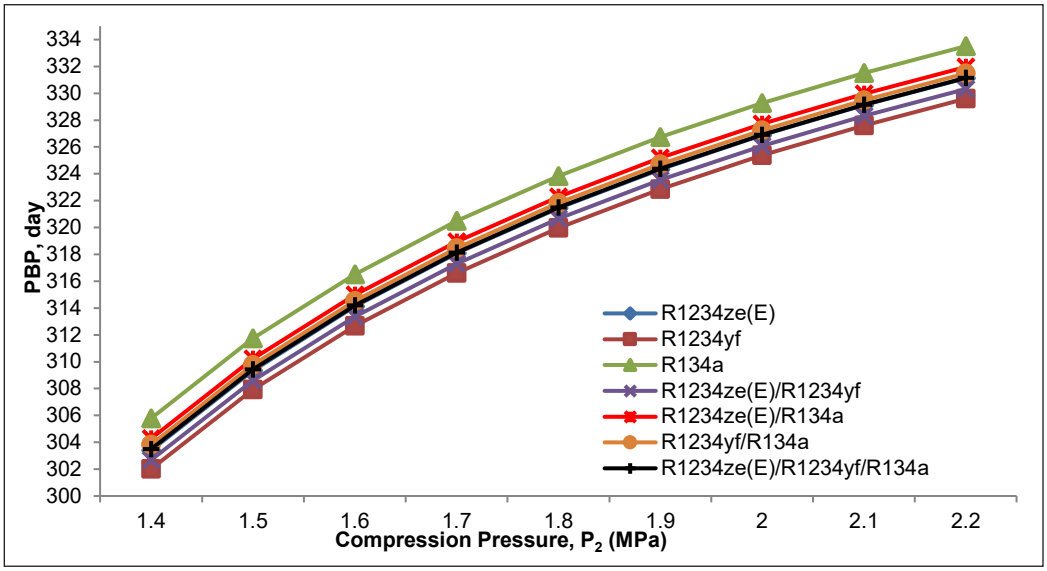

Figure 14. The payback period (PBP) of SORC system at different compression pressures of R1234ze(E), R1234yf, R134a, R1234ze(E)/R1234yf, R1234ze(E)/R134a, R1234yf/R134a, and R1234ze(E)/R1234yf/R134a as working fluids

and highest PBP of the SORC system belongs to the R1234yf and R134a with 302-330 and 306-333 days, respectively. Moreover, followed by them the R1234ze(E)/R1234yf, R1234ze(E)/R1234yf/R134a, R1234ze(E), R1234yf/R134a, and R1234ze(E)/R134a locate between these lowest to highest PBP of the SORC system. It is essential to say that these achievements are similar to the results of Li et al. (2019), Yang (2018), and Zhang et al. (2017).

CONCLUSION

In a nutshell, this study focused on designing, modeling, simulating, conducting, analyzing, and evaluating the Subcritical Organic Rankine Cycle (SORC), which is driven by pure, fixed binary and ternary zeotropic working fluids such as; R1234ze(E), R1234yf, R134a, R1234ze(E)/R1234yf (0.5/0.5), R1234ze(E)/R134a (0.5/0.5), R1234yf/R134a (0.5/0.5), and R1234ze(E)/R1234yf/R134a (0.4/0.3/0.3), respectively. Also, try to apply the flue gas (220°C), released from industrial boilers, as a heat source with medium temperature, open kind, and no restriction of the outlet temperature of the heat source in the evaporation process. Furthermore, a heat sink (cold water) and try to model, design, and simulation by utilizing the AspenPlus (v10), Simulink of Matlab (vR2017a), and REFPROP (v10) to analyze and achieve the optimum value of the thermo-physical and thermo-economic parameters based on compression pressure (1.4-2.2 MPa) as the main boundary condition. The main conclusions are made as follows.

Increasing the compression pressure has a positive relationship with the superheated temperature and the mass enthalpy change in the evaporation. Therefore, in the expansion process, the flue gas enthalpy change significantly affects the heat absorption capacity of the SORC system. This parameter is directly related to the mass enthalpy change in the evaporation and, therefore, in the expansion process of each working fluid as an effective parameter to generate optimum turbine power output (>1MW) of each working fluid. The highest and optimum range of the SORC net power output is 1283.22–2822.04 KW when R134a is adapted. Also, the lowest and optimum range of net power output belongs to R1234yf with only a 14.62–15.24% reduction. Likewise, R1234ze(E)/R134a, R1234yf/R134a, R1234ze(E)/R1234yf/R134a, R1234ze(E), and R1234ze(E)/R1234yf find out between the highest to lowest range of net power output, respectively.

The result of optimum exergy efficiency establishes that the R1234yf/R134a with 69.29% as the highest and the lowest exergy efficiency in the highest compression pressure of the present SORC system belongs to R1234ze(E)/R1234yf/R134a with only 0.94% reduction, compare with R1234yf/R134a is selected. Furthermore, it notes that the enthalpy and entropy changes in the flue gas and cold water have a positive relationship with exergy efficiency.

Considering the thermo-economic efficiency parameters, the SIC increases the cost of each component of the SORC system because of a similar trend to the PPC and in parallel with the required exchanger area and the net power generated by the turbine. As a result, the power consumes by the pump significantly. Moreover, SIC reveals the same results as PBP of the SORC system. For example, the maximum value to minimum value of SIC based on increasing the compression pressure achieves R134a with 5807402.18-22455670.61 $\$.kW^{-1}$ and R1234yf with 16.82-17.38% reduction, respectively. On the other hand, the highest and lowest amount of PPC belongs to the R134a and R1234yf with 81.74-316.07 and 67.99-261.11 $\$.kW^{-1}.year^{-1}$, respectively. To sum up, the PBP shows the same result as SIC and PPC with 306-333 and 302-330 days, which achieve R134a and R1234yf investigated at different inlet turbine pressure.

Further research should focus on developing and performing the present ORC by designing an EES (Engineering Equation Solver) method for greater computational numeric focus to understand the current ORC errors better to conduct in nonfiction.

ACKNOWLEDGEMENT

The authors want to acknowledge the financial support from Universiti Putra Malaysia via Geran Putra Matching (Matching Geran Putra/2019/9300467).

REFERENCES

Ahmadi, A., El Haj Assad, M., Jamali, D. H., Kumar, R., Li, Z. X., Salameh, T., Al-Shabi, M., & Ehyaei, M. A. (2020). Applications of geothermal Organic Rankine Cycle for electricity production. *Journal of Cleaner Production, 274*, Article 122950. https://doi.org/10.1016/j.jclepro.2020.122950

Alvi, J. Z., Feng, Y., Wang, Q., Imran, M., & Pei, G. (2021a). Effect of phase change materials on the performance of direct vapor generation solar Organic Rankine Cycle system. *Energy Reports, 223*, Article 120006. https://doi.org/10.1016/j.energy.2021.120006

Alvi, J. Z., Feng, Y., Wang, Q., Imran, M., & Pei, G. (2021b). Effect of working fluids on the performance of phase change material storage based direct vapor generation solar Organic Rankine Cycle system. *Energy Reports, 7*, 348-361. https://doi.org/10.1016/j.egyr.2020.12.040

Ata, S., Kahraman, A., & Sahin, R. (2020). Prediction and sensitivity analysis under different performance indices of R1234ze ORC with Taguchi's multi-objective optimization. *Case Studies in Thermal Engineering, 22*, Article 100785. https://doi.org/10.1016/j.csite.2020.100785

Bianchi, M., Branchini, L., De Pascale, A., Melino, F., Ottaviano, S., Peretto, A., & Torricelli, N. (2020). Replacement of R134a with low-GWP fluids in a kW-size reciprocating piston expander: Performance prediction and design optimization. *Energy, 206*, Article 118174. https://doi.org/10.1016/j.energy.2020.118174

Braimakis, K., Mikelis, A., Charalampidis, A., & Karellas, S. (2020). Exergetic performance of CO_2 and ultra-low GWP refrigerant mixtures as working fluids in ORC for waste heat recovery. *Energy, 203*, Article 117801. https://doi.org/10.1016/j.energy.2020.117801

Cambi, M., Tascioni, R., Cioccolanti, L., & Bocci, E. (2016). Converting a commercial scroll compressor into an expander: Experimental and analytical performance evaluation. *Energy Procedia, 129*, 363-370. https://doi.org/10.1016/j.egypro.2017.09.234

Chagnon-Lessard, N., Mathieu-Potvin, F., & Gosselin, L. (2020). Optimal design of geothermal power plants: A comparison of single-pressure and dual-pressure Organic Rankine Cycles. *Geothermics, 86*, Article 101787. https://doi.org/10.1016/j.geothermics.2019.101787

Eyerer, S., Dawo, F., Wieland, C., & Spliethoff, H. (2020). Advanced ORC architecture for geothermal combined heat and power generation. *Energy, 205*, Article 117967. https://doi.org/10.1016/j.energy.2020.117967

Guo, H., Gong, M., & Sun, H. (2021). Performance analysis of a novel energy storage system based on the combination of positive and reverse Organic Rankine Cycles. *Energy, 231*, Article 120905. https://doi.org/10.1016/j.energy.2021.120905

Hamid, M. R. A., Yaw, T. C. S., Tohir, M. Z. M., Ghani, W. A. W. A. K., Sutrisna, P. D., & Jeong, H. K. (2021). Zeolitic imidazolate framework membranes for gas separations: Current state-of-the-art, challenges, and opportunities. *Journal of Industrial and Engineering Chemistry, 98*, 17-41.

Hu, S., Li, J., Yang, F., Yang, Z., & Duan, Y. (2020). Multi-objective optimization of Organic Rankine Cycle using hydrofluorolefins (HFOs) based on different target preferences. *Energy, 203*, Article 117848. https://doi.org/10.1016/j.energy.2020.117848

Imran, M., Haglind, F., Asim, M., & Zeb Alvi, J. (2018). Recent research trends in Organic Rankine Cycle technology: A bibliometric approach. *Renewable and Sustainable Energy Reviews, 81*, 552-562. https://doi.org/10.1016/j.rser.2017.08.028

Invernizzi, C. M., Iora, P., Preßinger, M., & Manzolini, G. (2016). HFOs as substitute for R-134a as working fluids in ORC power plants: A thermodynamic assessment and thermal stability analysis. *Applied Thermal Engineering, 103*, 790-797. https://doi.org/10.1016/j.applthermaleng.2016.04.101

Ji, W. T., Xiong, S. M., Chen, L., Zhao, C. Y., & Tao, W. Q. (2021). Effect of subsurface tunnel on the nucleate pool boiling heat transfer of R1234ze(E), R1233zd(E) and R134a. *International Journal of Refrigeration, 122*, 122-133. https://doi.org/10.1016/j.ijrefrig.2020.11.002

Kang, Z., Zhu, J., Lu, X., Li, T., & Wu, X. (2015). Parametric optimization and performance analysis of zeotropic mixtures for an Organic Rankine Cycle driven by low-medium temperature geothermal fluids. *Applied Thermal Engineering, 89*, 323-331. https://doi.org/10.1016/j.applthermaleng.2015.06.024

Kavathia, K., & Prajapati, P. (2021). A review on biomass-fired CHP system using fruit and vegetable waste with regenerative Organic Rankine Cycle (RORC). *Materialstoday: Proceedings, 43*, 572-578. https://doi.org/10.1016/j.matpr.2020.12.052

Li, J., Liu, Q., Ge, Z., Duan, Y., & Yang, Z. (2017). Thermodynamic performance analyses and optimization of subcritical and transcritical Organic Rankine Cycles using R1234ze(E) for 100-200 °C heat sources. *Energy Conversion and Management, 149*, 140-154. https://doi.org/10.1016/j.enconman.2017.06.060

Li, L., Ge, Y. T., Luo, X., & Tassou, S. A. (2018). Experimental analysis and comparison between CO_2 transcritical power cycles and R245fa Organic Rankine Cycles for low-grade heat power generations. *Applied Thermal Engineering, 136*, 708-717. https://doi.org/10.1016/j.applthermaleng.2018.03.058

Li, T., Meng, N., Liu, J., Zhu, J., & Kong, X. (2019). Thermodynamic and economic evaluation of the Organic Rankine Cycle (ORC) and two-stage series organic Rankine cycle (TSORC) for flue gas heat recovery. *Energy Conversion and Management, 183*, 816-829. https://doi.org/10.1016/j.enconman.2018.12.094

Liu, P., Shu, G., Tian, H., Feng, W., Shi, L., & Wang, X. (2020). Experimental study on transcritical Rankine cycle (TRC) using CO_2/R134a mixtures with various composition ratios for waste heat recovery from diesel engines. *Energy Conversion and Management, 208*, Article 112574. https://doi.org/10.1016/j.enconman.2020.112574

Loni, R., Najafi, G., Bellos, E., Rajaee, F., Said, Z., & Mazlan, M. (2021). A review of industrial waste heat recovery system for power generation with Organic Rankine Cycle: Recent challenges and future outlook. *Journal of Cleaner Production, 287*, Article 125070. https://doi.org/10.1016/j.jclepro.2020.125070

Lu, P., Luo, X., Wang, J., Chen, J., Liang, Y., Yang, Z., Wang, C., & Chen, Y. (2021). Thermo-economic design, optimization, and evaluation of a novel zeotropic ORC with mixture composition adjustment during operation. *Energy Conversion and Management, 230*, Article 113771. https://doi.org/10.1016/j.enconman.2020.113771

Manente, G., Lazzaretto, A., & Bonamico, E. (2017). Design guidelines for the choice between single and dual pressure layouts in Organic Rankine Cycle (ORC) systems. *Energy, 123*, 413-431. https://doi.org/10.1016/j.energy.2017.01.151

Mignard, D. (2014). Correlating the chemical engineering plant cost index with macroeconomic indicators. *Chemical Engineering Research and Design, 92*(2), 285-294. https://doi.org/10.1016/j.cherd.2013.07.022

Molés, F., Navarro-Esbrí, J., Peris, B., Mota-Babiloni, A., & Mateu-Royo, C. (2017). R1234yf and R1234ze as alternatives to R134a in Organic Rankine Cycles for low temperature heat sources. *Energy Procedia, 142*, 1192-1198. https://doi.org/10.1016/j.egypro.2017.12.380

Nafey, A. S., & Sharaf, M. A. (2010). Combined solar organic Rankine cycle with reverse osmosis desalination process: energy, exergy, and cost evaluations. *Renewable Energy, 35*(11), 2571-2580. https://doi.org/10.1016/j.renene.2010.03.034

Peris, B., Navarro-Esbrí, J., Moles, F., Martí, J. P., & Mota-Babiloni, A. (2015). Experimental characterization of an Organic Rankine Cycle (ORC) for micro-scale CHP applications. *Applied Thermal Engineering, 79*, 1-8. https://doi.org/10.1016/j.applthermaleng.2015.01.020

Ping, X., Yang, F., Zhang, H., Zhang, J., Zhang, W., & Song, G. (2021). Introducing machine learning and hybrid algorithm for prediction and optimization of multistage centrifugal pump in an ORC system. *Energy, 222*, Article 120007. https://doi.org/10.1016/j.energy.2021.120007

Quoilin, S., Declaye, S., Tchanche, B. F., & Lemort, V. (2011). Thermo-economic optimization of waste heat recovery Organic Rankine Cycles. *Applied Thermal Engineering, 31*(14-15), 2885-2893. https://doi.org/10.1016/j.applthermaleng.2011.05.014

Roumpedakis, T. C., Loumpardis, G., Monokrousou, E., Braimakis, K., Charalampidis, A., & Karellas, S. (2020). Exergetic and economic analysis of a solar driven small scale ORC. *Renewable Energy, 157*, 1008-1024. https://doi.org/10.1016/j.renene.2020.05.016

Rowshanaie, O., Mustapha, S., Ahmad, K. A., & Rowshanaie, H. (2015). Simulation of Organic Rankine Cycle through flue gas to large scale electricity generation purpose. *Jurnal Teknologi, 77*(27), 9-18. https://doi.org/10.11113/jt.v77.6878

Rowshanaie, O., Tohir, M. Z. M., Mustapha, F., Ya'acob, M. E., & Rowshanaie, H. (2020). Optimization and analyzing of subcritical Organic Rankine Cycle using R1234ze(E) for low and medium temperature heat source. *IOP Conf. Series: Materials Science and Engineering, 778*, Article 012074. https://doi.org/10.1088/1757-899X/778/1/012074

Schilling, J., Entrup, M., Hopp, M., Gross, J., & Bardow, A. (2021). Towards optimal mixtures of working fluids: Integrated design of processes and mixtures for Organic Rankine Cycles. *Renewable and Sustainable Energy Reviews, 135*, Article 110179. https://doi.org/10.1016/j.rser.2020.110179

Shengjun, Z., Huaixin, W., & Tao, G. (2011). Performance comparison and parametric optimization of subcritical Organic Rankine Cycle (ORC) and transcritical power cycle system for low-temperature geothermal power generation. *Applied Energy, 88*(8), 2740-2754. https://doi.org/10.1016/j.apenergy.2011.02.034

Sun, K., Zhao, T., Wu, S., & Yang, S. (2021). Comprehensive evaluation of concentrated solar collector and Organic Rankine cycle hybrid energy process with considering the effects of different heat transfer fluids. *Energy Reports, 7*, 362-384. https://doi.org/10.1016/j.egyr.2021.01.004

Sun, Q., Lin, D., Khayatnezhad, M., & Taghavi, M. (2021). Investigation of phosphoric acid fuel cell, linear Fresnel solar reflectorand Organic Rankine Cycle polygeneration energy system in different climatic

conditions. *Process Safety and Environmental Protection, 147*, 993-1008. https://doi.org/10.1016/j.psep.2021.01.035

Tian, R., Xu, Y., Shi, L., Song, P., & Wei, M. (2020). Mixed convection heat transfer of supercritical pressure R1234yf in horizontal flow: Comparison study as alternative to R134a in organic Rankine cycles. *Energy, 205*, Article 118061. https://doi.org/10.1016/j.energy.2020.118061

Turton, R., Bailie, R. C., Whiting, W. B., Shaeiwitz, J. A., & Bhattacharyya, D. (2012). *Analysis, synthesis and design of chemical processes* (4th Ed.). Pearson Education.

Vaupel, Y., Huster, W. R., Mhamdi, A., & Mitsos, A. (2021). Optimal operating policies for Organic Rankine Cycles for waste heat recovery under transient conditions. *Energy, 224*, Article 120126. https://doi.org/10.1016/j.energy.2021.120126

Vélez, F., Segovia, J. J., Martín, M. C., Antolín, G., Chejne, F., & Quijano, A. (2012). A technical, economical and market review of Organic Rankine Cycles for the conversion of low-grade heat for power generation. *Renewable and Sustainable Energy Reviews, 16*(6), 4175-4189. https://doi.org/10.1016/j.rser.2012.03.022

Vera, D., Baccioli, A., Jurado, F., & Desideri, U. (2020). Modeling and optimization of an ocean thermal energy conversion system for remote islands electrification. *Renewable Energy, 162*, 1399-1414. https://doi.org/10.1016/j.renene.2020.07.074

Wang, F., Wang, L., Zhang, H., Xia, L., Miao, H., & Yuan, J. (2021). Design and optimization of hydrogen production by solid oxide electrolyzer with marine engine waste heat recovery and ORC cycle. *Energy Conversion and Management, 229*, Article 113775. https://doi.org/10.1016/j.enconman.2020.113775

Wang, J., Wang, J., Li, J., & Liu, N. (2020). Pressure drop of R134a and R1234ze(E) flow boiling in microchannel arrays with single- and double-side heating. *International Journal of Heat and Mass Transfer, 161*, Article 120241. https://doi.org/10.1016/j.ijheatmasstransfer.2020.120241

Wang, Z., Xia, X., Pan, H., Zuo, Q., Zhou, N., & Xie, B. (2021). Fluid selection and advanced exergy analysis of dual-loop ORC using zeotropic mixture. *Applied Thermal Engineering, 185*, Article 116423. https://doi.org/10.1016/j.applthermaleng.2020.116423

Yang, F., Zhang, H., Song, S., Bei, C., Wang, H., & Wang, E. (2015). Thermoeconomic multi-objective optimization of an Organic Rankine Cycle for exhaust waste heat recovery of a diesel engine. *Energy, 93*, 2208-2228. https://doi.org/10.1016/j.energy.2015.10.117

Yang, M. H. (2018). Payback period investigation of the Organic Rankine Cycle with mixed working fluids to recover waste heat from the exhaust gas of a large marine diesel engine. *Energy Conversion and Management, 162*, 189-202. https://doi.org/10.1016/j.enconman.2018.02.032

Yang, Z., Valtz, A., Coquelet, C., Wu, J., & Lu, J. (2020). Experimental measurement and modelling of vapor-liquid equilibrium for 3,3,3- Trifluoropropene (R1243zf) and trans-1,3,3,3-Tetrafluoropropene (R1234ze(E)) binary system. *International Journal of Refrigeration, 120*, 137-149. https://doi.org/10.1016/j.ijrefrig.2020.08.016

Yu, X., Huang, Y., Li, Z., Huang, R., Ghang, J., & Wang, L. (2021). Characterization analysis of dynamic behavior of basic ORC under fluctuating heat source. *Applied Thermal Engineering, 189*, Article 116695. https://doi.org/10.1016/j.applthermaleng.2021.116695

Zhai, H., An, Q., & Shi, L. (2016). Analysis of the quantitative correlation between the heat source temperature and the critical temperature of the optimal pure working fluid for subcritical Organic Rankine Cycles. *Applied Thermal Engineering, 99*, 383-391. https://doi.org/10.1016/j.applthermaleng.2016.01.058

Zhai, H., An, Q., & Shi, L. (2018). Zeotropic mixture active design method for Organic Rankine Cycle. *Applied Thermal Engineering, 129*, 1171-1180. https://doi.org/10.1016/j.applthermaleng.2017.10.027

Zhang, C., Fu, J., Kang, J., & Fu, W. (2018). Performance optimization of low-temperature geothermal organic Rankine cycles using axial turbine isentropic efficiency correlation. *Journal of the Brazilian Society of Mechanical Sciences and Engineering, 40*, Article 61. https://doi.org/10.1007/s40430-018-0996-9

Zhang, C., Liu, C., Wang, S., Xu, X., & Li, Q. (2017). Thermo-economic comparison of subcritical organic Rankine cycle based on different heat exchanger configurations. *Energy, 123*, 728-741. https://doi.org/10.1016/j.energy.2017.01.132

Zhang, Y., Lei, B., Masaud, Z., Imran, M., Wu, Y., Liu, J., Qin, X., & Muhammad, H. A. (2020). Waste heat recovery from diesel engine exhaust using a single-screw expander Organic Rankine Cycle system: Experimental investigation of exergy destruction. *Energies, 13*(22), Article 5914. https://doi.org/10.3390/en13225914

Zheng, N., Wei, J., & Zhao, L. (2018). Analysis of a solar Rankine cycle powered refrigerator with zeotropic mixtures. *Solar Energy, 162*, 57-66. https://doi.org/10.1016/j.solener.2018.01.011